Mathematical Modeling of Myosin Induced Bistability of Lamellipodial Fragments

S. Hirsch[*], A. Manhart[†], C. Schmeiser[‡]

March 2, 2016

Abstract

For various cell types and for lamellipodial fragments on flat surfaces, externally induced and spontaneous transitions between symmetric nonmoving states and polarized migration have been observed. This behavior is indicative of bistability of the cytoskeleton dynamics. In this work, the Filament Based Lamellipodium Model (FBLM), a two-dimensional, anisotropic, two-phase continuum model for the dynamics of the actin filament network in lamellipodia, is extended by a new description of actin-myosin interaction. For appropriately chosen parameter values, the resulting model has bistable dynamics with stable states showing the qualitative features observed in experiments. This is demonstrated by numerical simulations and by an analysis of a strongly simplified version of the FBLM with rigid filaments and planar lamellipodia at the cell front and rear.

Keywords: Actin, Mathematical Model, Cytoskeleton

Acknowledgments: Financial support by the Austrian Science Fund (FWF) through the doctoral school Dissipation and Dispersion in Nonlinear PDEs (project W1245, S.H./A.M.) as well as the Vienna Science and Technology Fund (WWTF) (project LS13/029, C.S.)

[*]Faculty of Mathematics, University of Vienna, Oskar-Morgenstern-Platz 1, 1090 Vienna, Austria, Tel. +431427750718, Email: stefanie.hirsch@univie.ac.at

[†]Faculty of Mathematics, University of Vienna, Oskar-Morgenstern-Platz 1, 1090 Vienna, Austria, Email: angelika.manhart@univie.ac.at

[‡]Faculty of Mathematics, University of Vienna, Oskar-Morgenstern-Platz 1, 1090 Vienna, Austria, Email: christian.schmeiser@univie.ac.at

1 Introduction

In a variety of physiological processes such as wound healing, immune response, or embryonic development, crawling cells play a vital role [1]. Cell motility is the result of an interplay between protrusion at the 'front' edge of the cell (w.r.t. the direction of movement), retraction at the rear, as well as translocation of the cell body [29]. It only occurs when the cell is polarized with a front and a differently shaped rear [8].

In this work we concentrate on cells on flat substrates, where both protrusion and retraction involve the so-called *lamellipodium*, a thin, sheet-like structure along the perimeter of a cell, consisting of a meshwork of *actin filaments*. F-actin is a polar dimer that forms inextensible filaments with a fast-growing plus (barbed) end and a slow-growing minus (pointed) end [6]. In the lamellipodium the filament network is approximately two-dimensional as opposed to the situation in several types of motile cells where protrusion is driven by fully three-dimensional actin networks.

The barbed ends abut on the membrane at the leading edge [18] and have a high probability of polymerization (i.e. elongation of the filament by insertion of new actin monomers), whereas at the pointed ends mostly depolymerization (removal of one monomer) or disassembly of larger parts through severing of the filament occurs. Once a balance between polymerization and depolymerization is reached, each incorporated monomer is being pushed back by newly added monomers. Using the filament itself as a frame of reference, this can be described as movement of monomers from the barbed end towards the pointed end, a process called *treadmilling* (see [15] and the references therein for an overview of the involved processes and proteins). New filaments are nucleated predominantly by branching off existing filaments. The resulting meshwork is an (almost) two-dimensional array of (almost) diagonally arranged actin filaments with decreasing density towards the cell body [28, 37].

The lamellipodium is stabilized by the cell membrane (surrounding the entire cell [17, 34]), adhesions to the substrate [13, 24], cross-linking proteins [19, 27] and myosin II filaments [31], the latter two binding to pairs of filaments. Some of the long filaments from the lamellipodium extend into the region behind, where (through the contractile effect of myosin II) forces are generated which pull the lamellipodium backwards [29].

Fish epidermal keratocytes are fast-moving cells with a relatively simple shape (circular, when stationary and crescent-moon-shaped, when moving [12]), which makes them ideal subjects for analysis. Furthermore, they exhibit a lamellipodium with a smooth edge and a fairly uniform distribution of filaments [10, 29, 32]. During the transition from the stationary to the moving state, the lamellipodium in the rear of the cell collapses and the *rear bundle* is formed, where myosin II generates a contractile force [31, 33, 35].

Treatment with staurosporine (a protein kinase inhibitor) results in the formation of completely detached lamellipodial fragments, lacking a cell body, microtubules and most other cell organelles. Remarkably, these fragments can either remain stationary while adopting a circular shape, or can move on their own, adapting their appearance to the same crescent-moon shape as the keratocyte itself [8, 36] (see Figure 1A-C). This suggests that the necessary ingredients for movement are all present in the lamellipodium (until it runs out of energy).

Various approaches to continuum mechanical modeling of the lamellipodium exist (see e.g. [9, 26]). Bistability results similar to this work have been obtained in [39], where a phase-field approach is used to describe the interplay between the cell shape, the mean orientation of the filaments within the network and the actin-myosin interaction. A strongly simplified model is developed in [8], where bistability has been obtained analytically as the consequence of the

Figure 1: A: a moving keratocyte (right) and a moving cytoplast (left), actin is labelled in green, the nucleus in blue. B and C: a moving and a stationary cytoplast (fragment), respectively. The actin network is labelled in red, myosin in green. A, B and C are reproduced from [14]. E: idealization with protruding lamellipodium at the top and lamellipodium collapsed by actin-myosin interaction at the bottom. D: model ingredients of the simplified FBLM (clockwise, starting top left): cross-link stretching, cross-link twisting, filament-substrate adhesion, connection between front and rear by stress fibres, membrane stretching, actin-myosin interaction.

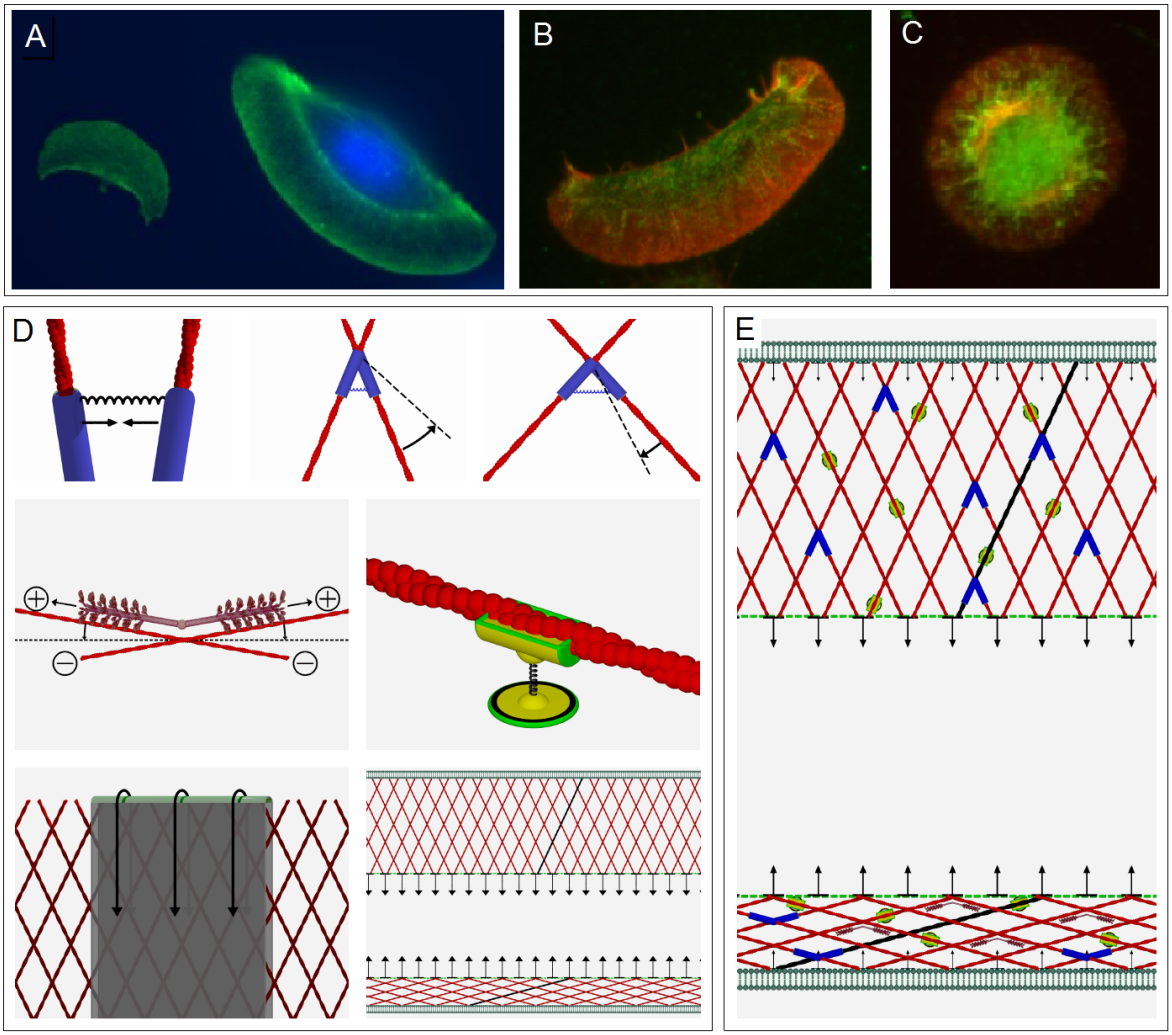

properties of a free energy functional containing contributions from the lamellipodium and a possible rear bundle.

This work is based on the FBLM [15, 21, 22], a two-dimensional, anisotropic, two-phase model derived from a microscopic (i.e. individual filament based) description, accounting for most of the phenomena mentioned above. It describes the actin network in terms of two transversal families of locally parallel filaments, stabilized by transient cross-links and substrate adhesions. In Section 2 the FBLM is presented and extended by a model for actin-myosin interaction between the two families. We assume that myosin filaments can connect

only when the families are anti-parallel enough and they are described as transient, similar to cross-links. They tend to slide the two families relative to each other, and they are assumed to have a turning effect, making the two families more anti-parallel. The derivation of the additional myosin terms is presented in detail. Readers not consulting [15, 21, 22] may take this as representative also for the derivation of the adhesion and cross-link models.

The properties of the actin-myosin model are expected to produce the desired bistable behavior. This is demonstrated by numerical simulations in Section 8, which indicate the existence of two stable states, a rotationally symmetric nonmoving state and a polarized state, where the cell moves. The moving state is characterized by a more anti-parallel network in the rear of the cell, where actin-myosin interaction is active. Complete collapse of the network and consequential generation of a rear bundle are avoided, since the FBLM is (so far) unable to deal with such topological changes.

The occurrence of bistability is also proven analytically for a strongly simplified model. In Section 3 the complexity of the model is reduced in a first step by assuming rigid filaments. Then a planar, translationally invariant lamellipodium is considered in Section 4, which reduces the model to a system of three ordinary differential equations. Here we also neglect the effects of branching and capping, assumed to be in equilibrium, as well as filament severing within the modelled part of the lamellipodium, implying a constant actin density there. Bistability is obtained for this model in Section 5. Finally, in Section 6 a cell (fragment) is replaced by a pair of connected back-to-back planar lamellipodia, and the existence of stable stationary (symmetric) as well as moving (polarized) states is proven. The same bistable behavior is observed in the simulations of the full model in Section 8.

Figure 1 depicts the main components of the simplified version of the FBLM (D and E) together with one keratocyte and three fragments (A-C). The crescent-moon shaped cells and cell fragments are moving, whereas the circularly shaped fragment remains stationary. One can also observe that in moving fragments myosin can predominantly be found at the cell rear. In Figure 1E, the idealized model obtained in Sections 3-6 is illustrated. It can be interpreted as description of lamellipodial sections at the front and at the rear of the cell. The main model ingredients are depicted in 1D: diagonally arranged filaments (red), the cell membrane (green, with arrows indicating the force acting on the barbed ends due to membrane tension), cross-links (blue, producing friction between the filament families and a turning force trying to establish an equilibrium angle), adhesions (yellow, producing friction relative to the substrate), myosin filaments (pink, trying to slide the filament families and to make them anti-parallel), and the inward pulling forces due to stress fibers in the interior of the cell (dashed green line and arrows).

2 Adding actin-myosin interaction to the Filament Based Lamellipodium Model (FBLM)

Our starting point is the FBLM as introduced in [21] (see also [15]):

$$\begin{aligned} 0 \;=\; & \mu^B \partial_s^2 \left(\eta \partial_s^2 F\right) + \mu^A \eta D_t F - \partial_s \left(\eta \lambda_{\text{inext}} \partial_s F\right) \\ & + \widehat{\mu^S} \eta\eta^* (D_t F - D_t^* F^*) \pm \partial_s \left(\widehat{\mu^T} \eta\eta^* (\varphi - \varphi_0) \partial_s F^\perp\right) , \end{aligned} \tag{1}$$

where $F = F(\alpha, s, t) \in \mathbb{R}^2$ describes the position and deformation of actin filaments in the plane at time t. More precisely, the variable $\alpha \in A \subset \mathbb{R}$, for some interval A, is a filament

label, and $s \in [-L(\alpha,t),0]$ denotes an arclength parameter along filaments, which means that the constraint

$$|\partial_s F| = 1 \tag{2}$$

has to be satisfied. Here $L(\alpha,t)$ is the maximal length of filaments in an infinitesimal region $d\alpha$ around α. The filament length density with respect to α and s is given by $\eta(\alpha,s,t)$, which will be assumed as given (see [15] for a dynamic model incorporating polymerization, depolymerization, nucleation, and branching effects). The value $s = 0$ corresponds to the so called *barbed ends* of the polar filaments, abutting the leading edge of the lamellipodium. The rear boundary $s = -L(\alpha,t)$ is introduced somewhat artificially since the rear end of the lamellipodium is typically not well defined. By polymerization with speed $v(\alpha,t)$ (also assumed as given in this work), monomers move along filaments in the negative s-direction. Their speed relative to the nonmoving substrate is therefore given by $D_t F$ with the material derivative $D_t = \partial_t - v\partial_s$.

The terms in the first line of (1) correspond to the filaments' resistance against bending with stiffness parameter μ^B, to friction relative to the substrate as a consequence of adhesion dynamics with adhesion coefficient μ^A, and to the constraint (2) with the Lagrange multiplier λ_{inext}.

The FBLM is actually a two phase model, and F may stand for either of the two families F^+ or F^-. The terms in the second line of (1) describe the interaction between the two families, with the other family indicated by the superscript $*$. The interaction is the consequence of dynamic cross-linking and leads to a friction term proportional to the relative velocity between the two families and to a turning force trying to push the angle φ ($\cos\varphi = \partial_s F \cdot \partial_s F^*$) between crossing filaments to its equilibrium value φ_0, corresponding to the equilibrium conformation of the cross-linker molecule ($F^\perp = (-F_y, F_x)$). The $*$-quantities corresponding to the other family have to be evaluated at (α^*, s^*), determined by the requirement $F(\alpha,s,t) = F^*(\alpha^*,s^*,t)$. It is a basic geometric modeling assumption that the coordinate change $(\alpha,s) \leftrightarrow (\alpha^*,s^*)$ is one-to-one, wherever the two families overlap. It requires that filaments of the same family do not cross each other and that pairs of filaments of different families cross each other at most once. Finally, the coefficients are given by

$$\widehat{\mu^S} = \mu^S \left|\frac{\partial\alpha^*}{\partial s}\right|, \qquad \widehat{\mu^T} = \mu^T \left|\frac{\partial\alpha^*}{\partial s}\right|, \tag{3}$$

with constants $\mu^{S,T}$, wherever F crosses another filament, and zero elsewhere. The partial derivative refers to the coordinate transformation introduced above.

The FBLM will be extended by the effects of myosin polymers. The basic assumption is that pairs of crossing actin filaments, which lie antiparallel enough, may be connected by a bipolar myosin filament. The modeling is similar to that of cross-links and we will give details of the derivation of the myosin related term (originally presented in [14]) as an example of the general modeling strategy of the FBLM. We assume the following about myosin molecules:

- Myosin filaments connect pairs of crossing actin filaments.
- Due to the motor activity of the myosin heads they "walk" towards the barbed ends of actin filaments with a fixed speed v^M.
- The rates of creation and breakage of the myosin connections depend on the forces acting on them (see below).

- The connections exert twisting forces on the connected actin filaments towards the equilibrium angle π, i.e. the antiparallel state. These forces are caused by the stiffness of myosin filaments.
- The connections can be stretched against an elastic restoring force.

The key to the bistability results presented in the next sections is the assumption that the myosin activity (specified below) depends on the angle between crossing actin filaments. This is supported by data reported in [25], where it has been shown that myosin can act much more efficiently on antiparallel actin networks as opposed to branched networks. In the original model of the myosin dynamics presented in [14], the growth of myosin filaments was also included. Here, we omit myosin size effects for the sake of simplicity. The derivation is done in five steps.

Step 1: Energy Contributions. Let a filament with label α have a crossing with a filament from the other family with label α^*. By $s(\alpha, \alpha^*, t)$ we denote the s-position along the α-filament where this crossing occurs. If at time $t-a$ a myosin filament has been attached at this crossing (i.e. the connection has age a at time t), the s-value of the binding site will change due to the aforementioned treadmilling effect (caused by actin polymerization) and the myosin motor activity. Therefore at time t the myosin filament binds to the actin filament at

$$s_a(\alpha, \alpha^*, t) = s(\alpha, \alpha^*, t-a) - \int_{t-a}^{t} \left(v(\alpha, \tilde{t}) - v^M\right) d\tilde{t}\,. \tag{4}$$

Analogously, the position $s_a^*(\alpha, \alpha^*, t)$ at time t of the binding site on the α^*-filament is computed. With the aid of s_a and s_a^* we can now determine the deviations from the unstretched and untwisted equilibrium state of the myosin filament:

$$\begin{aligned}
&S_a^M(\alpha, \alpha^*, t) = F\left(\alpha, s_a(\alpha, \alpha^*, t), t\right) - F^*\left(\alpha^*, s_a^*(\alpha, \alpha^*, t), t\right),\\
&T_a^M(\alpha, \alpha^*, t) = \varphi_a(\alpha, \alpha^*, t) - \pi, \qquad \text{where}\\
&\cos(\varphi_a(\alpha, \alpha^*, t)) = \partial_s F\left(\alpha, s_a(\alpha, \alpha^*, t), t\right) \cdot \partial_s F^*\left(\alpha^*, s_a^*(\alpha, \alpha^*, t), t\right).
\end{aligned}$$

Note that $S_0^M = 0$ and $T_0^M = \varphi - \pi$, i.e. the myosin filament is unstretchted but possibly bent at the time a connection is created.

Now let $\rho^M(\alpha, \alpha^*, a, t)$ denote the probability density with respect to age a of an active myosin connection between the filaments with label α and α^* at time t. Following classical modeling for age-structured populations we assume ρ^M to satisfy

$$\begin{aligned}
&\partial_t \rho^M + \partial_a \rho^M = -\zeta(S_a^M, T_a^M)\rho^M,\\
&\rho^M(a=0) = \beta(T_0^M)\left(1 - \int_0^\infty \rho^M d\tilde{a}\right).
\end{aligned}$$

The rate of breakage ζ may depend on the stretching and twisting forces acting on the myosin filament. We also allow for the possibility that the rate of creation β is affected by how favorable the angle between the actin filaments is. The interpretation of the last factor is that a new connection can only connect a so far unconnected pair of actin filaments.

The main equation (1) of the FBLM is the result of a variational approach applied to the problem of minimizing a sum of potential energies. Each energy contribution produces forces

acting on the actin filament (i.e. bending stiffness, adhesions, etc.). To include new terms, it is therefore necessary to formulate the corresponding energy. For the elastic stretching and twisting of the myosin filaments, we choose the form

$$U^M_{\text{stretching}}[F, F^*] = \int_0^\infty \int_{\mathcal{C}(t-a)} \frac{\kappa^{SM}}{2} \left|S^M_a\right|^2 \rho^M \eta\eta^* d(\alpha, \alpha^*) da,$$
$$U^M_{\text{twisting}}[F, F^*] = \int_0^\infty \int_{\mathcal{C}(t-a)} \frac{\kappa^{TM}}{2} (T^M_a)^2 \rho^M \eta\eta^* d(\alpha, \alpha^*) da.$$

The integration domain $\mathcal{C}(t-a)$ includes all pairs of filaments (α, α^*), which had a crossing at time $t-a$. The constants κ^{SM} and κ^{TM} are elasticity coefficients.

Step 2: Scaling. The key scaling assumption of the original FBLM is that the average lifetime of a cross-link or adhesion is small compared to the average time a monomer spends inside a filament, a ratio denoted by ε. In the limit $\varepsilon \to 0$ the non-locality in time is removed from the problem. Furthermore this reduces the effect of adhesions to friction with the substrate and that of the cross-linkers to friction between the filament families (compare eq. (1)).

This raises the question of what to assume about the average lifetime of a myosin filament. In [31] it was observed that in stationary cytoplasts myosin spots stay small and disappear after some time, indicating their transient nature. The situation is quite different for moving cytoplasts, where the myosin spots grow in size over time. Since the aim of this paper is to describe the onset of movement, we use here the same scaling assumption as for cross-links, i.e. that the lifetime of a myosin filament is relatively short. Without going into further detail about the precise reference values for all variables and parameters, we state the resulting energy contributions and equations after scaling: The density equations take the form

$$\varepsilon \partial_t \rho^M_\varepsilon + \partial_a \rho^M_\varepsilon = -\zeta(S^M_{\varepsilon a}, T^M_{\varepsilon a}) \rho^M_\varepsilon,$$
$$\rho^M_\varepsilon(a=0) = \beta(T^M_0) \left(1 - \int_0^\infty \rho^M_\varepsilon d\tilde{a}\right).$$

Since $S^M_{\varepsilon a} \to 0$ and $T^M_{\varepsilon a} \to T^M_0 = \varphi - \pi$ as $\varepsilon \to 0$, we can explicitly calculate the solution to the limiting equation. In the following we will replace dependencies on T^M_0 by dependencies on φ. Ignoring a possible initial time layer, the limiting solution is given by

$$\rho^M_0 = \frac{\beta(\varphi)\zeta(0,\varphi)}{\beta(\varphi) + \zeta(0,\varphi)} e^{-\zeta(0,\varphi)a}. \tag{5}$$

Note that ρ^M_0 depends on t and the indices α and α^* via the angle between the filaments.

The scaled energy contributions take the form

$$U^M_{\text{stretching}}[F, F^*] = \frac{1}{\varepsilon} \int_0^\infty \int_{\mathcal{C}(t-\varepsilon a)} \frac{\kappa^{SM}}{2} \left|S^M_{a\varepsilon}\right|^2 \rho^M_\varepsilon \eta\eta^* d(\alpha, \alpha^*) da,$$
$$U^M_{\text{twisting}}[F, F^*] = \int_0^\infty \int_{\mathcal{C}(t-\varepsilon a)} \frac{\kappa^{TM}}{2} (T^M_{\varepsilon a})^2 \rho^M_\varepsilon \eta\eta^* d(\alpha, \alpha^*) da.$$

The factor $1/\varepsilon$ in front of the stretching contribution is the result of a scaling assumption. It ensures that the effect of myosin filament stretching does not vanish in the limit, although the energy contribution itself does.

Step 3: Variation and macroscopic limit. The next step in the derivation is to calculate the variations $\delta U[F, F^*]\delta F$ of the energy contributions, considering ρ_ε^M given at this stage. After passing to the limit $\varepsilon \to 0$, we obtain

$$\delta U^M_{\text{stretching}}[F, F^*]\,\delta F = \int_{\mathcal{C}(t)} \mu^{SM}\left(D_t^M F - D_t^{M*}F^*\right)\cdot \delta F\,\eta\eta^* d(\alpha,\alpha^*),$$
$$\delta U^M_{\text{twisting}}[F, F^*]\,\delta F = \int_{\mathcal{C}(t)} \mu^{TM}\left(\partial_s F^\perp \cdot \partial_s \delta F\right)(\varphi-\pi)\eta\eta^* d(\alpha,\alpha^*),$$

where $D_t^M F$ denotes the velocity of a myosin binding site on the actin filament relative to the substrate, with

$$D_t^M := \partial_t - (v - v^M)\partial_s.$$

The stiffness parameters μ^{SM} and μ^{TM} result from using the representation of ρ_0^M given in (5) to evaluate the integrals with respect to the myosin age a. They take the form

$$\mu^{SM}(\varphi) = \frac{\beta(\varphi)\kappa^{SM}}{\zeta(0,\varphi)\left(\beta(\varphi)+\zeta(0,\varphi)\right)}, \qquad \mu^{TM}(\varphi) = \frac{\beta(\varphi)\kappa^{TM}}{\beta(\varphi)+\zeta(0,\varphi)}.$$

Motivated by the findings in [25], we assume that there exists a cutoff angle $\overline{\varphi} < \pi$ such that

$$\mu^{SM}(\varphi) = \mu^{TM}(\varphi) = 0 \qquad \text{for} \quad \varphi < \overline{\varphi} < \pi\,.$$

Step 4: Euler-Lagrange Equations. The final step in the derivation is to formulate the corresponding Euler-Lange equations. Together with the original terms given in (1), the modified model takes the form

$$\begin{aligned} 0 \;=\; & \mu^B\partial_s^2\left(\eta\partial_s^2 F\right) + \mu^A\eta D_t F - \partial_s\left(\eta\lambda_{\text{inext}}\partial_s F\right) \\ & + \widehat{\mu^S}\eta\eta^*(D_t F - D_t^* F^*) \pm \partial_s\left(\widehat{\mu^T}\eta\eta^*(\varphi-\varphi_0)\partial_s F^\perp\right) \\ & + \widehat{\mu^{SM}}\eta\eta^*(D_t^M F - D_t^{M*}F^*) \pm \partial_s\left(\widehat{\mu^{TM}}\eta\eta^*(\varphi-\pi)\partial_s F^\perp\right), \end{aligned} \tag{6}$$

with

$$\widehat{\mu^{SM}} = \mu^{SM}(\varphi)\left|\frac{\partial\alpha^*}{\partial s}\right|, \qquad \widehat{\mu^{TM}} = \mu^{TM}(\varphi)\left|\frac{\partial\alpha^*}{\partial s}\right|, \tag{7}$$

The introduction of $\widehat{\mu^{SM}}$ and $\widehat{\mu^{TM}}$ is a consequence of the mapping between $\mathcal{C}$ and $\{(\alpha, s) : \alpha \in A, s \in [-L(\alpha,t), 0]\}$. Further details of the model derivation can be found in [14].

Step 5: Boundary conditions describe the forces acting on the filaments at their barbed ends and at the artificially introduced ends at the boundary of the modeling domain:

$$\begin{aligned} & \mu^B\partial_s\left(\eta\partial_s^2 F\right) - \eta\lambda_{\text{inext}}\partial_s F \pm \widehat{\mu^T}\eta\eta^*(\varphi-\varphi_0)\partial_s F^\perp \pm \widehat{\mu^{TM}}\eta\eta^*(\varphi-\pi)\partial_s F^\perp = -f_0\,, \\ & \partial_s^2 F = 0\,, \qquad \text{for } s = 0\,. \\ & \mu^B\partial_s\left(\eta\partial_s^2 F\right) - \eta\lambda_{\text{inext}}\partial_s F \pm \widehat{\mu^T}\eta\eta^*(\varphi-\varphi_0)\partial_s F^\perp \pm \widehat{\mu^{TM}}\eta\eta^*(\varphi-\pi)\partial_s F^\perp = f_L\,, \\ & \partial_s^2 F = 0\,, \qquad \text{for } s = -L\,. \end{aligned} \tag{8}$$

Thus, there are no torques applied at the ends. The choice of the linear forces f_0 and f_L along the leading edge and, respectively, along the artificial boundary will be discussed later.

3 Rigid actin filaments in the limit of large bending stiffness

We want to derive a simplified model with rigid actin filaments. This is motivated on the one hand by the observation that filaments within the lamellipodium are typically rather straight [37]. On the other hand stiff filaments can be interpreted as a description of only the outermost part of the lamellipodial region, where filaments are (locally) straight. The resulting model is mathematically much simpler and can be derived by assuming a relatively large bending stiffness μ^B. The limit $\mu^B \to \infty$ will be carried out formally in this section.

The solutions of the formal limit

$$0 = \partial_s^2 \left(\eta \partial_s^2 F\right)$$

of (6), together with the boundary conditions

$$\partial_s^2 F = 0\,, \qquad \text{for } s = 0, -L\,,$$

and with the constraint (2), can be written as

$$F(\alpha, s, t) = F_0(\alpha, t) + (s - s_0(\alpha, t)) d(\omega(\alpha, t))\,, \qquad \text{with } d(\omega) = \begin{pmatrix} \cos\omega \\ \sin\omega \end{pmatrix}, \tag{9}$$

where s_0 is determined by

$$\int_{-L}^{0} \eta(\alpha, s, t)(s - s_0(\alpha, t)) ds = 0\,.$$

In other words, F_0 is the center of mass of the filament, and $d(\omega)$ its direction. The components of F_0 and the angle ω are still to be determined. The total force balance obtained by integration of (6) with respect to s and using the boundary conditions (8) reads

$$\begin{aligned} f_0 + f_L = \int_{-L}^{0} \Big(& \mu^A \eta D_t F + \widehat{\mu^S} \eta\eta^* (D_t F - D_t^* F^*) \\ & + \widehat{\mu^{SM}} \eta\eta^* (D_t F - D_t^* F^* + v^M(\partial_s F - \partial_s F^*)) \Big) ds\,. \end{aligned} \tag{10}$$

Note that it does not contain μ^B and therefore remains valid in the limit. Similarly, the total torque balance is obtained by integration of (6) against $(F - F_0)^\perp$:

$$\begin{aligned} & (F - F_0)^\perp(s = 0) \cdot f_0 + (F - F_0)^\perp(s = -L) \cdot f_L \\ & \quad = \mp \int_{-L}^{0} \widehat{\mu^T} \eta\eta^* (\varphi - \varphi_0) ds \mp \int_{-L}^{0} \widehat{\mu^{TM}} \eta\eta^* (\varphi - \pi) ds \\ & \qquad + \int_{-L}^{0} (F - F_0)^\perp \cdot \Big(\mu^A \eta D_t F + \widehat{\mu^S} \eta\eta^* (D_t F - D_t^* F^*) \\ & \qquad + \widehat{\mu^{SM}} \eta\eta^* (D_t F - D_t^* F^* + v^M(\partial_s F - \partial_s F^*)) \Big) ds\,. \end{aligned} \tag{11}$$

This completes the formulation of the rigid filament version of the FBLM. Substitution of (9) into (10) and (11) gives a system of ordinary differential equations for F_0 and ω. Note that coupling with respect to α happens only indirectly through the interaction between the two filament families.

4 A geometric simplification: the planar lamellipodium

Since in keratocytes the leading edge is rather smooth, we approximate a piece of lamellipodium by an infinite strip, parallel to the x-axis, and invariant to translations and to reflection. For the given data this means that the maximal filament length L and the polymerization speed v are constants. As a further simplification, we assume no filament ends inside the modeled part of the lamellipodium with the consequence $\eta = 1$ (and $s_0 = -L/2$).

We assume two families of rigid filaments (9) with

$$\begin{aligned} F_0^+(\alpha^+, t) &= \begin{pmatrix} x(t) + \alpha^+ \\ y(t) \end{pmatrix}, \quad \alpha^+ \in \mathbb{R}\,, \qquad \omega^+(\alpha^+, t) = \omega(t) \in [0, \pi/2]\,, \\ F_0^-(\alpha^-, t) &= \begin{pmatrix} -x(t) + \alpha^- \\ y(t) \end{pmatrix}, \quad \alpha^- \in \mathbb{R}\,, \qquad \omega^-(\alpha^-, t) = \pi - \omega(t) \in [\pi/2, \pi]\,, \end{aligned}$$

giving

$$F^\pm(\alpha^\pm, s^\pm, t) = \begin{pmatrix} \pm x(t) + \alpha^\pm \pm (s^\pm + L/2)\cos\omega(t) \\ y(t) + (s^\pm + L/2)\sin\omega(t) \end{pmatrix}, \qquad \alpha^\pm \in \mathbb{R}\,, \quad s^\pm \in [-L, 0]\,.$$

The angle between two crossing filaments and the coordinate change between the two families mentioned in Section 2 are easily computed:

$$\varphi = \pi - 2\omega, \qquad \alpha^- = \alpha^+ + 2x(t) + (2s^+ + L)\cos\omega(t)\,, \qquad s^- = s^+\,.$$

It provides the geometric quantity needed in (3) and (7):

$$\left|\frac{\partial \alpha^-}{\partial s^+}\right| = 2\cos\omega\,.$$

This quantity can be interpreted as a measure of the density of crossings, with a maximum at $\omega = 0$ (fully collapsed lamellipodium) and a minimum at $\omega = \pi/2$ (all filaments are parallel, no crossings).

With the planar lamellipodium ansatz, the equations (10) and (11) become independent of α and constitute a system of three ordinary differential equations for the unknowns $(x(t), y(t), \omega(t))$:

$$\begin{aligned} \dot{x}\left[\mu^A + 4(\mu^S + \mu^{SM}(\pi - 2\omega))\cos\omega\right] &= \frac{f_{0,x} + f_{L,x}}{L} + \mu^A v\cos\omega + 4\mu^S v\cos^2\omega \\ &\quad + 4\mu^{SM}(\pi - 2\omega)(v - v^M)\cos^2\omega\,, \qquad (12) \\ \dot{y}\mu^A &= \frac{f_{0,y} + f_{L,y}}{L} + \mu^A v\sin\omega\,, \qquad (13) \\ \dot{\omega}\left[\mu^A + 4\sin^2\omega\cos\omega(\mu^S + \mu^{SM}(\pi - 2\omega))\right] &= \frac{6}{L^2} d(\omega)^\perp \cdot (f_0 - f_L) \\ &\quad + \frac{24}{L^2}\mu^T(\pi - 2\omega - \varphi_0)\cos\omega \\ &\quad - \frac{48}{L^2}\mu^{TM}(\pi - 2\omega)\omega\cos\omega\,. \qquad (14) \end{aligned}$$

5 Forces at the filament ends – steady protrusion

The membrane stretched around the lamellipodium exerts a force on the polymerizing barbed ends. On the other hand, we assume that the filaments at the rear of the lamellipodium are connected to stress fibres pulling them backwards, another consequence of actin-myosin interaction. Both the membrane force and the stress fibre force will be described as acting in the negative y-direction orthogonal to the leading edge, i.e.

$$f_{0,x} = f_{L,x} = 0\,, \qquad f_{0,y} = -f_{mem}\,, \qquad f_{L,y} = -f_{stress}\,. \tag{15}$$

If these forces are modeled as constant, the equation (14) for the angle is decoupled from the remaining system. For an analysis of its dynamic behavior, we choose a model for the stiffness coefficients of the actin-myosin connection:

$$\mu^{SM}(\varphi) = \overline{\mu^{SM}}\,(\varphi - \overline{\varphi})_+\,, \qquad \mu^{TM}(\varphi) = \overline{\mu^{TM}}\,(\varphi - \overline{\varphi})_+\,, \tag{16}$$

with $\overline{\mu^{SM}}, \overline{\mu^{TM}} > 0$, $\varphi_0 < \overline{\varphi} < \pi$, and with the notation $(.)_+$ for the positive part.

Bistability can now be obtained with appropriate assumptions on the parameters. The right hand side of (14) can be written as

$$\frac{24}{L^2}\cos\omega\left(\frac{f_{stress} - f_{mem}}{4} + h(\omega)\right) \qquad \text{with } h(\omega) = \mu^T(\pi - 2\omega - \varphi_0) - 2\omega\overline{\mu^{TM}}(\pi - 2\omega - \overline{\varphi})_+\,.$$

It is a simple exercise to prove:

Lemma 1. If

$$\frac{\overline{\mu^{TM}}}{\mu^T} > \frac{\overline{\varphi} + \pi - 2\varphi_0 + 2\sqrt{(\pi - \varphi_0)(\overline{\varphi} - \varphi_0)}}{(\pi - \overline{\varphi})^2}, \tag{17}$$

then $h(\omega)$ as defined above has three simple zeroes ω_{10}, ω_{20}, ω_{30}, satisfying

$$\frac{\pi}{2} > \omega_{10} = \frac{\pi - \varphi_0}{2} > \frac{\pi - \overline{\varphi}}{2} > \omega_{20} > \omega_{30} > 0\,.$$

Theorem 2. Under the assumptions of Lemma 1 and for $|f_{stress} - f_{mem}|$ small enough, the ordinary differential equation (14) with the forces given by (15) possesses four stationary solutions ω_j, $j = 0, \ldots, 3$ with

$$\omega_0 = \pi/2 > \omega_1 = \frac{\pi - \varphi_0}{2} + \frac{f_{stress} - f_{mem}}{8\mu^T} > \frac{\pi - \overline{\varphi}}{2} > \omega_2 > \omega_3 > 0\,,$$

where ω_0 and ω_2 are unstable, and ω_1 and ω_3 are asymptotically stable.

Again the proof is straightforward. For the stable steady states, the lamellipodium has the constant protrusion speeds

$$\dot{y} = v\sin\omega_{1,3} - \frac{f_{stress} + f_{mem}}{\mu^A L}\,.$$

For the equilibrium angle ω_1, we typically expect the speed to be positive. It is not affected by actin-myosin interaction. The smaller speed corresponding to ω_3 might actually be

negative due to membrane tension and stress fibres, i.e. the second stable state, where the lamellipodium is collapsed by actin-myosin interaction, might be retractive.

Finally, the steady states also produce lateral flow with constant speeds

$$\dot{x} = v\cos\omega_1 \qquad \text{and} \qquad \dot{x} = \left(v - v^M \frac{4\mu^{SM}\cos\omega_3}{\mu^A + 4\mu^S\cos\omega_3 + 4\mu^{SM}\cos\omega_3}\right)\cos\omega_3\,,$$

respectively, where in the collapsed state the lateral flow speed produced by polymerization is reduced by actin-myosin interaction.

6 Coupling of two opposing lamellipodia – bistability

As a caricature of a cell fragment, we consider two back-to-back planar lamellipodia (see Figure 1E). For notational convenience, the bottom lamellipodium is rotated by 180^o in the mathematical description. Therefore we consider two versions of the system (12)–(14) with unknowns (x, y, ω) and $(\hat{x}, \hat{y}, \hat{\omega})$. The assumption that the total forces exerted on the fragment by membrane tension and by stress fibres vanish, imply that (15) is used in both systems with the same values for f_{mem} and f_{stress}. However, we allow the option that these forces are not constant but regulate the size of the fragment, measured by $y + \hat{y}$. We first consider the case of a constant given membrane force and a size dependent force by stress fibres:

$$\textbf{Case A:} \qquad f_{mem} = \text{const}\,, \quad f_{stress} = f_{stress}(y + \hat{y})\,.$$

Typically f_{stress} will be an increasing function, but the details are not important for our considerations.

Adding the equations (13) for y and $\hat{y}$ leads to a closed system of three equations for $y+\hat{y}$, ω, and $\hat{\omega}$:

$$(\dot{y} + \dot{\hat{y}})\mu^A = -\frac{2}{L}(f_{mem} + f_{stress}(y + \hat{y})) + \mu^A v(\sin\omega + \sin\hat{\omega})\,, \tag{18}$$

$$\dot{\omega}\, g(\omega) = \cos\omega\left(\frac{f_{stress}(y + \hat{y}) - f_{mem}}{4} + h(\omega)\right)\,, \tag{19}$$

$$\dot{\hat{\omega}}\, g(\hat{\omega}) = \cos\hat{\omega}\left(\frac{f_{stress}(y + \hat{y}) - f_{mem}}{4} + h(\hat{\omega})\right)\,, \tag{20}$$

with

$$g(\omega) = \frac{L^2}{24}\left[\mu^A + 4\sin^2\omega\cos\omega(\mu^S + \mu^{SM}(\pi - 2\omega))\right]\,.$$

We shall prove that with appropriate assumptions on the data, the problem has 4 stable steady states.

Theorem 3. Let the assumptions of Lemma 1 hold, let the function f_{stress} be continuously differentiable with bounded positive derivative, and let f_{mem}, $\mu^A vL$, and the Lipschitz constant of f_{stress} be small enough. Then the system (18)–(20) has four stable steady states, satisfying

$$\omega = \hat{\omega} = \omega_{\mathrm{CL}}\,, \tag{21}$$

$$\omega = \hat{\omega} = \omega_{\mathrm{MY}}\,, \tag{22}$$

$$\omega = \omega_{\mathrm{CL}}\,, \quad \hat{\omega} = \omega_{\mathrm{MY}}\,, \tag{23}$$

$$\omega = \omega_{\mathrm{MY}}\,, \quad \hat{\omega} = \omega_{\mathrm{CL}}\,, \tag{24}$$

where the purely cross-link dominated state ω_{CL} and the myosin-influenced state ω_{MY} are given by:

$$\omega_{\mathrm{CL}} := \omega_{10} + O(f_{mem} + \mu^A v L)\,,$$
$$\omega_{\mathrm{MY}} := \omega_{30} + O(f_{mem} + \mu^A v L)\,.$$

Proof. From (18) we obtain that steady states have to satisfy

$$f_{stress}(y+\hat{y}) = -f_{mem} + \frac{\mu^A L v}{2}(\sin\omega + \sin\hat{\omega})\,. \tag{25}$$

This implies, again for stable steady states, $h(\omega) = h(\hat{\omega}) = O(f_{mem} + \mu^A v L)$. The existence of the four steady states is then a consequence of a straightforward perturbation argument. The coefficient matrix in the linearization of (18)–(20) can be written as

$$\begin{pmatrix} -2\kappa/(\mu^A L) & v\cos\omega & v\cos\hat{\omega} \\ A\kappa & Ah'(\omega) & 0 \\ \hat{A}\kappa & 0 & \hat{A}h'(\hat{\omega}) \end{pmatrix},$$

with positive constants A and $\hat{A}$, and with $0 < \kappa = f'_{stress}(y+\hat{y}) \ll 1$. A perturbation analysis of the eigenvalue problem for small κ (i.e. formal expansion of eigenvalues in terms of powers of κ and subsequent justification by a contraction argument) gives the eigenvalues

$$\lambda_1 = Ah'(\omega) + O(\kappa)\,, \quad \lambda_2 = \hat{A}h'(\hat{\omega}) + O(\kappa)\,, \quad \lambda_3 = \kappa\left(-\frac{2}{\mu^A L} + \frac{v\cos\omega}{h'(\omega)} + \frac{v\cos\hat{\omega}}{h'(\hat{\omega})}\right) + O(\kappa^2)\,,$$

which are all negative at the four steady states for small enough κ, because of $h'(\omega_{10}), h'(\omega_{30}) < 0$. □

For the steady states the protrusion speed of the fragment is constant and given by

$$\dot{y} = -\dot{\hat{y}} = \frac{v}{2}(\sin\omega - \sin\hat{\omega})\,. \tag{26}$$

For the symmetric steady states (21), (22), the protrusion speeds vanish, hence they describe stationary cells (or fragments). The equilibrium angles in the lamellipodia in this case are either both affected by myosin, (22), or both result only from cross-link activity, (21). The asymmetric steady states (23) and (24) describe a protruding, polarized cell. In both cases it consists of a collapsed cell rear, in which myosin is active ($\omega = \omega_{\mathrm{MY}}$), and a cell front with a steeper equilibrium angle caused only by cross-link activity ($\omega = \omega_{\mathrm{CL}}$).

Finally, we also mention the case of a constant stress fibre force and a size dependent membrane force:

$$\textbf{Case B:} \qquad f_{stress} = \mathrm{const}\,, \quad f_{mem} = f_{mem}(y+\hat{y})\,.$$

Without going through the details, we note that the qualitative results are the same and a theorem analogous to Theorem 3 can be proven.

7 Parameter dependencies

The simplifications of the two preceding sections lead to several (testable) statements. This section can be seen as a discussion of the results so far.

Protrusion speed vs. adhesion strength: For the coupled lamellipodium of Section 6 the protrusion speed is given by (26). For a moving fragment, i.e. situation (23) or (24), we compute

$$\frac{d(\sin\omega_{\mathrm{CL}} - \sin\omega_{\mathrm{MY}})}{d\mu^A} = \left(\cos\omega_{\mathrm{CL}} - \frac{d\omega_{\mathrm{MY}}}{d\omega_{\mathrm{CL}}}\cos\omega_{\mathrm{MY}}\right)\frac{d\omega_{\mathrm{CL}}}{d\mu^A}\,.$$

Substitution of (25) into the stationary version of (19) (resp. (20)) shows that $d\omega_{\mathrm{CL}}/d\mu^A > 0$. On the other hand, the difference of the stationary versions of (19) and (20) gives $d\omega_{\mathrm{MY}}/d\omega_{\mathrm{CL}} < 0$. Thus, the protrusion speed increases with adhesion strength. Since the results of Theorem 3 are restricted to relatively small adhesiveness, this is in agreement with experimental results [2] showing two regimes: For smaller adhesion strengths the cell speed is positively correlated with the adhesiveness of the ground. After reaching a maximum speed, the correlation is reversed for larger adhesion strengths.

It is not clear if the FBLM in its present form is able to describe the second regime, which might be caused by long-lived focal adhesions, contradicting the assumption of rapid adhesion turnover. It should also be noted that it has been hypothesized (see [2]) that the reduction of cell speed on strongly adhesive ground is mainly due to biochemical reasons as opposed to purely mechanical effects.

Onset of myosin activity: The inequality (17) gives a criterion for the existence of a myosin influenced stable steady state. Myosin has to be strong enough compared to forces maintaining the branched actin network structure (e.g. Arp2/3, filamin, etc.). Only then is it able – either spontaneously or aided by a pushing force – to initiate the collapse of the network, which precedes bundle formation. Data like those presented in [25] show that myosin activitiy is influenced by actin network structure. The model for myosin activity (16), used for the analyis in this work, can be interpreted as a limiting case, in which the activity is set to zero for unfavorable angles. From the approximation

$$\overline{\mu^{TM}}(\pi - \overline{\varphi})^2 > 4\mu^T(\pi - \varphi_0)$$

of (17) for $\overline{\varphi}$ close to π, it is easily seen that if the interval for the myosin angle is small, this needs to be compensated by a large stiffness of the myosin filament in order to initiate symmetry breaking. In our model myosin is necessary for the onset of movement, i.e. polarization of originally symmetric fragments. In [38] the number of stationary cells spontaneously initiating motility within a given time interval was reduced from 45% to 10% by inhibiting myosin using blebbistatin, which supports our findings.

Protrusion speed vs. myosin strength: In the presented model two parameters characterize myosin strength, the elasticity coefficients of myosin filament stretching $\overline{\mu^{SM}}$ and bending $\overline{\mu^{TM}}$. Whereas $\overline{\mu^{SM}}$ has no influence on the equilibrium angle and therefore also not on the protrusion speed, larger values of $\overline{\mu^{TM}}$ lead to faster cells (easily seen in the expression for $h(\omega)$). This is consistent with experimental results found in [2] where myosin contraction was either inhibited using blebbistatin (leading to slower cells at least for low to medium adhesion strengths) or enhanced using calyculin A (leading to faster cells in all adhesive regimes).

8 Simulations with the full model

In this section we demonstrate that with the additional term describing myosin within the lamellipodium, the model is able to produce cells/cell fragments that, depending on the initial conditions, will either remain stationary or start moving. In contrast to the simulations presented in [15] and [16], here the movement is achieved without a continuing external signal and without varying the polymerization speed. In the simulation, we work with the full model (6)–(8) and not with the simplifications introduced in Sections 3 and 4. However, the qualitative results of Section 6 will be reproduced.

Parameter values: Parameter values are chosen as in [15] with the following exceptions and additions: we work with a constant filament density $\eta = 1$ in parameter space, which means that the filament number remains constant with branching and capping always in equilibrium. No pointed ends appear within the simulation region, which corresponds to a fixed filament length of $L = 8\mu m$. The polymerization speed is fixed at the constant value $v = 3\mu m\,\mathrm{min}^{-1}$. In [31] it has been observed that myosin speckles that are formed in the lamellipodium drift inwards with time. This indicates that the myosin velocity has to be smaller than the polymerization speed. We therefore chose $v^M = 1\mu m\,\mathrm{min}^{-1}$. Motivated by [25] we assume that myosin can only act on actin filaments if the angle between the filaments is larger than $\overline{\varphi} = 100°$. For the stiffness parameters of stretching and twisting the cross-links and myosin good estimates are hard to obtain, since their exact concentration in the lamellipodium is difficult to determine. Motivated by Lemma **??** we chose the myosin twisting force larger than the cross-link twisting force (see Table 1), but of the same order of magnitude. Additionally we increased the bending stiffness by a factor 10 in order to get closer to the analytical case examined in Sections 3. Here we concentrated on the case of size control via stress fiber forces from the inside, i.e. the membrane force was set to zero. The stress fiber force was chosen to be $f_{stress} = \mu^{IP}(A - A_0)_+$, where A is the current size of the area surrounded by the lamellipodium, A_0 is the equilibrium inner area and μ^{IP} is the corresponding (inner pulling) force constant. In order not to distort the direction of the filaments, we let the stress fibers pull only tangentially on the pointed ends. The numerical parameters are chosen as in [15], i.e. 36 discretization nodes in α direction and 9 nodes in s-direction. The timestep used is 2×10^{-3}min.

Figure 2: Cell view with clockwise filaments in blue and anti-clockwise filaments in red. Green stars in the lamellipodium mark the area where myosin is active. The black dot marks the origin, the black star the cell's center of mass. The insets show the angles between the filaments of the different families, averaged along each filament, parametrized along the membrane with 0 being at the very right and going counterclockwise. Blue (dashed) lines refer to the clockwise filament family, red (solid) lines to the anti-clockwise filament family. The horizontal green line at 100° marks the myosin cut-off value $\overline{\varphi}$. A–D: Time series with $\mu^{TM} = 1.4\times10^{-2} pN\,\mu m$. Myosin is initially active in the left part of the cell, but is not strong enough to stay there. Eventually the cell goes back to the stationary cross-link dominated equilibrium. E–H: Time series with $\mu^{TM} = 1.8\times10^{-2} pN\,\mu m$. Myosin is initially active in the left part of the cell, where a myosin/cross-link equilibrium emerges. Since the right of the cell is unaffected by this, the cell moves to the right. Parameters as in Table 1.

Simulation results: Figure 2 shows the evolution of the cell in two different numerical experiments over a timespan of 15 minutes. In both cases identical initial conditions were used,

in which the left side of the cell is deformed. This could be caused either by internal fluctuations or by a pushing force from the left, two situations known to lead to symmetry breaking in fragments [36]. Both simulations use the same set of parameters, with the exception of the value of the myosin twisting constant, μ^{TM}, which is smaller in the left column than in the right column. In Figure 2A–D it can be observed that even though the filaments on the left initially lie anti-parallel enough for myosin to act on them, myosin does not establish itself there permanently. Lemma 1 gives a possible explanation for this: If myosin is too weak compared to the cross-links, there is no myosin/cross-link-equilibrium, hence the cell reverts back to a purely cross-link dominated state. This situation corresponds to the steady state (21) in Theorem 3.
The case of a larger myosin twisting constant is depicted in Figure 2E–H: In situation case a bundle-precursor is formed on the left, whereas the right stays myosin free. This allows the cell to change to a moving steady state (see the Supplementary Material for a movie) with a collapsed lamellipodium at the back and a non-collapsed lamellipodium at the front, a situation described by the steady states (23) and (24) in Theorem 3. One can also observe the contraction of the rear bundle leading to a more half-moon shaped cell. Clearly if the initial deformations are so small that no myosin can attach, the cell always reverts back to the stationary state. This refers to a situation where the fluctuations or pushing force are too small to cause symmetry breaking.

9 Discussion and Outlook

In this work, we extended the FBLM introduced in [15, 21] by a description of actin-myosin interaction. The limit of large bending stiffness led to a simplified model for rigid filaments. The additional simplification of a planar lamellipodium reduces the model to a small ODE system for the center of mass of a reference filament and the angle with the membrane. A caricature of a cell fragment has been described by considering two versions of the model coupled by membrane and stress fiber forces. Bistability has been shown in the asymptotic regime of relatively small coupling forces and adhesion strength. Since these results are almost explicit, various parameter dependencies could be obtained. Furthermore, we carried out numerical simulations based on the full FBLM supporting the main analytical result of bistable behaviour.

Our model is able to qualitatively reproduce the observed bistability of cells and cell fragments [36]. Since myosin has been shown to be effective only if the angle between the filaments is large enough [25], our specific modeling of the myosin effect to be angle-dependent seems to be a reasonable choice.

In the numerical simulations we have shown that for an initially slightly asymmetric cell, one of two stable steady states is attained, depending on the parameters for myosin and cross-links. If myosin is too weak to exert considerable twisting forces, the effects from cross-links on the local angles between the filaments dominate and the cell reverts back to a symmetric nonmoving shape. On the other hand, if myosin forces are strong enough, a bundle precursor forms at the 'rear' (the location of initial asymmetry), and the cell starts moving. What is apparent in these simulations is that myosin tends to locate at the back of the lamellipodium (away from the membrane). This is also in good agreement with experimental findings. It is remarkable that both for the analytical setting as well as in the numerical simulations, movement is an self-organized behavior, once an initial asymmetry has been established. It

Table 1: Parameter Values

Var.	Meaning	Value	Comment
L	filament length	$8\mu m$	order of magnitude as in [36]
A_0	equilibrium inner area	$300\mu m^2$	order of magnitude as in [36]
N	total filament number	9000	order of magnitude as in [7]
μ^B	bending elasticity	$0.7pN\mu m^2$	10 times higher than in [3]
μ^A	macroscopic friction caused by adhesions	$0.14pN\text{min}\mu m^{-2}$	measurements in [13, 20], estimation and calculations in [23, 22, 21]
v	polymerization speed	$3\mu m\,\text{min}^{-1}$	in biological range
φ_0	equilibrium cross-link angle	70°	equal to the branching angle
μ^S	cross-link stretching constant	$4.2\times10^{-3}pN\,min\,\mu m^{-1}$	
μ^T	cross-link twisting constant	$4.2\times10^{-3}pN\,\mu m$	
v^M	myosin velocity	$1\mu m\,\text{min}^{-1}$	order of magnitudes as in [31]
$\overline{\varphi}$	myosin cut-off	100°	
$\overline{\mu^{SM}}$	myosin stretching constant	$4.2\times10^{-3}pN\,\text{min}\,\mu m^{-1}$	
$\overline{\mu^{TM}}$	myosin twisting constant	$1.4\times10^{-2}pN\,\mu m$	motivated by Lemma 1, Simulation 1
		$1.8\times10^{-2}pN\,\mu m$	motivated by Lemma 1, Simulation 2
μ^{stress}	stress fiber force	$5\times10^{-2}pN\mu m^{-1}$	

is known that keratocytes exhibit little if any chemotaxis, i.e. directed movement to outward cues.

An important issue remains to be addressed: The analytical model, dealing only with pieces of lamellipodium at the front and at the rear of the cell, avoids the transition zone separating the two parts of the lamellipodium with an intact network on the one hand and, on the other hand, compression to a rear bundle. It can be expected that due to lateral flow, actin filaments are drawn into the bundle in these transition regions. However, we expect that this happens with the pointed ends first entering the bundle, as opposed to the simulations presented here. A model supporting the necessary change of orientation in the transition zone is not available so far, and its derivation is the subject of ongoing work.

References

[1] R. Ananthakrishnan, A. Ehrlicher, The forces behind cell movement, *Int. J. of Biol. Sciences* **3** (2007), pp. 303–317.

[2] E.L. Barnhart, K.-C. Lee, K. Keren, A. Mogilner, J. Theriot, An adhesion-dependent switch between mechanisms that determine motile cell shape, *PLoS Biology* **9** (2011), pp. e1001059.

[3] F. Gittes, B. Mickey J. Nettleton, J. Howard, Flexural rigidity of microtubules and actin filaments measured from thermal fluctuations in shape, *J. Cell Biol.* **120** (1993), pp. 923–934.

[4] H.P. Grimm, A.B. Verkhovsky, A. Mogilner, J.-J. Meister, Analysis of actin dynamics at the leading edge of crawling cells: implications for the shape of keratocyte lamellipodia, *Eur. Biophys. J.* **32** (2003), pp. 563–577.

[5] W.H. Goldmann, G. Isenberg, Analysis of filamin and α-actinin binding to actin by the stopped flow method, *FEBS Letters* **336** (1993), pp. 408–410.

[6] K.C. Holmes, D. Popp, W. Gebhard, W. Kabsch, Atomic model of the actin filament, *Nature* **347** (1990), pp. 44–49.

[7] S.A. Koestler, S. Auinger, M. Vinzenz, K. Rottner, J.V. Small, Differentially oriented populations of actin filaments generated in lamellipodia collaborate in pushing and pausing at the cell front, *Nature Cell Biol.* **10** (2008), pp. 306–313.

[8] M.M. Kozlov, A. Mogilner, Model of polarization and bistability of cell fragments, *Biophys. J.* **93** (2007), pp. 3811–3819.

[9] K. Kruse, J.-F. Joanny, F. Julicher, P. Prost, Contractility and retrograde flow in lamellipodium motion, *Phys. Biol.* **3** (2006), pp. 130–137.

[10] C.I. Lacayo, Z. Pincus, M.M. VanDuijn, C.A. Wilson, D.A. Fletcher, F.B. Gertler, A. Mogilner, J.A. Theriot, Emergence of large-scale cell morphology and movement from local actin filament growth dynamics, *PLOS Biol.* **5** (2007), e233.

[11] K. Larripa, A. Mogilner, Transport of a 1D viscoelastic actin-myosin strip of gel as a model of a crawling cell, *Physica A* **372** (2006), pp. 113–123.

[12] J. Lee, A. Ishihara, J. Theriot, K. Jacobson, Principles of locomotion for simple-shaped cells, *Nature* **362** (1993), pp. 167–171.

[13] F. Li, S.D. Redick, H.P. Erickson, V.T. Moy, Force measurements of the $\alpha 5\beta 1$ integrin-bronectin interaction, *Biophys. J.* **84(2)** (2003), pp. 1252–1262.

[14] A. Manhart, *A Mathematical Model of Actin-Myosin Interaction and its Application to Keratocyte Movement,* Masters thesis, University of Vienna, 2011.

[15] A. Manhart, D. Oelz, N. Sfakianakis, C. Schmeiser, An extended Filament Based Lamellipodium Model produces various moving cell shapes in the presence of chemotactic signals, preprint, 2015.

[16] A. Manhart, D. Oelz, N. Sfakianakis, C. Schmeiser, Numerical treatment of the Filament Based Lamellipodium Model (FBLM), preprint, 2015.

[17] T.Mitchison, L.Cramer, Actin-based cell motility and cell locomotion, *Cell* **84** (1996), pp. 371–379.

[18] A. Mogilner, Mathematics of cell motility: have we got its number? *J. Math. Biol.* **58** (2009), pp.105–134.

[19] F. Nakamura, T.M. Osborn, C.A. Hartemink, J.H. Hartwig, T.P. Stossel, Structural basis of lamin A functions, *J. Cell Biol.* **179(5)** (2007), pp. 1011–1025.

[20] A.F. Oberhauser, C. Badilla-Fernandez, M. Carrion-Vazquez, J.M. Fernandez, The mechanical hierarchies of fibronectin observed with single-molecule AFM, *J. Mol. Biol.* **319(2)** (2002), pp.433–447.

[21] D. Ölz, C. Schmeiser, How do cells move? Mathematical modelling of cytoskeleton dynamics and cell migration, in *Cell mechanics: from single scale-based models to multiscale modelling,* eds. A. Chauviere, L. Preziosi, and C. Verdier, Chapman and Hall / CRC Press, 2010.

[22] D. Ölz, C. Schmeiser, Derivation of a model for symmetric lamellipodia with instantaneous cross-link turnover, *Archive Rat. Mech. Anal.* **198** (2010), pp. 963–980.

[23] D. Ölz, C. Schmeiser, J.V. Small, Modelling of the actin-cytoskeleton in symmetric lamellipodial fragments, *Cell Adhesion & Migration* **2** (2008), pp. 117-126.

[24] L.M. Pierini, M.A. Lawson, R.J. Eddy, B. Hendey, F.R. Maxeld, Oriented endocytic recycling of $\alpha\beta 1$ in motile neutrophils, *Blood* **95(8)** (2000), pp. 2471–2480.

[25] A. Reymann, et. al., Actin Network Architecture Can Determine Myosin Motor Activity, *Science* **336** (2012), pp. 1310–1314.

[26] B. Rubinstein, K. Jacobson, A. Mogilner, Multiscale two-dimensional modeling of a motile simple- shaped cell, *Multiscale Model. Simul.* **3** (2005), pp. 413–439.

[27] I. Schwaiger, A. Kardinal, M. Schleicher, A. Noegel, M. Rief, A mechanical unfolding intermediate in an actin-crosslinking protein, *Nature Structural and Molecular Biol.* **11(1)** (2004), pp. 81–85.

[28] J.V. Small, M.Herzog, K.Anderson, Actin filament organization in the fish keratocyte lamellipodium, *J. Cell Biol.* **129** (1995), pp. 1275–1286.

[29] J.V. Small, G.Resch, The comings and goings of actin: coupling protrusion and retraction in cell motility, *Curr. Opinion in Cell Biol.* **17** (2005), pp. 517–523.

[30] J.V. Small, T. Stradal, E. Vignal, K. Rottner, The lamellipodium: where motility begins, *Trends in Cell Biol.* **12** (2002), pp. 112–120.

[31] T.M. Svitkina, A. B. Verkhovsky, K.M. McQuade, G.G. Borisy, Analysis of the actin-myosin II system in fish epidermal keratocytes: mechanism of cell body translocation, *J. Cell Biol.* **139(2)** (1997), pp. 397–415

[32] J.A. Theriot, T.J. Mitchison, Actin microfilament dynamics in locomoting cells, *Nature* **352** (1991), pp.126–131.

[33] S. Tojkander, G. Gateva, P. Lappalainen, Actin stress fibers - assembly, dynamics and biological roles, *J. Cell Sci.*, **125(8)** (2012), pp. 1855-1864.

[34] P. Vallotton, G. Danuser, S. Bohnet, J.-J. Meister, A. B. Verkhovsky, Tracking retrograde flow in keratocytes: news from the front, *Mol. Biol. of the Cell* **16** (2005), pp. 1223–1231.

[35] A.B. Verkhovsky, T.M. Svitkina, G.G. Borisy, Polarity sorting of actin filaments in cytochalasin-treated fibroblast, *J. Cell Sci.* **110** (1997), pp. 1693–1704.

[36] A.B. Verkhovsky, T.M. Svitkina, G.G. Borisy, Self-polarization and directional motility of cytoplasm, *Curr. Biol.* **9** (1999), pp. 11–20.

[37] M. Vinzenz et al., Actin branching in the initiation and maintenance of lamellipodia, *J. Cell Sci.* **125** (2012), pp. 2775–2785.

[38] P. T. Yam et. al., Actin-myosin network reorganization breaks symmetry at the cell rear to spontaneously initiate polarized cell motility, *J. of Cell Biol.* **178** (2007), pp. 1207–1221.

[39] F. Ziebert, S. Swaminathan, I.S. Aranson, Model for self-polarization and motility of keratocyte fragments, *J. Royal. Soc. Interface* **9** (2012), pp. 1084–1092.